PCCP

Accepted Manuscript

ROYAL SOCIETY OF CHEMISTRY

www.rsc.org/pccp

Divergent trend in density *versus* viscosity of ionic liquid/water mixtures: A molecular view from guanidinium ionic liquids

Akhil Pratap Singh,[1,2] Ramesh Gardas,[2] and Sanjib Senapati[1,*]

[1]Bhupat and Jyoti Mehta School of Biosciences, Department of Biotechnology, [2]Department of Chemistry, Indian Institute of Technology Madras, Chennai 600036, India

Phone: +91-44-2257-4122. Fax: +91-44-2257-4102. E-mail: sanjibs@iitm.ac.in.

Abstract

Ionic liquids (ILs) have shown great potential in dissolution and stability of biomolecules when a low-to-moderate quantity of water is added. Hence, determining the thermophysical properties and understanding these novel mixtures at molecular level is of both fundamental and practical importance. In this context, here we report the synthesis of two nontoxic guanidinium cation based ILs, tetramethylguanidinium benzoate [TMG][BEN] and tetramethylguanidinium salicylate [TMG][SAL], and present a detailed comparison of their thermophysical properties in presence of water. Results show that the [TMG][SAL]/water mixtures have higher density and higher apparent molar volume, but a lower viscosity and higher compressibility than the [TNG][BEN]/water mixtures. The measured viscosity and compressibility data are explained from *ab initio* quantum mechanical calculations and liquid-phase molecular dynamics simulations, where salicylate anions of denser [TMG][SAL]/water was found to exist as isolated ions due to intramolecular H-bonding. On the contrary, intermolecular H-bonding among the benzoate anions and their strong tendency to form extended H-bonding network with water, made [TMG][BEN]/water solutions more viscous and less compressible. The study shows the importance of probing these emerging solvents at molecular-to-atomic level, which could be helpful in their optimal usage for task-specific applications.

1. INTRODUCTION

Ionic liquids (ILs) are organic salts with low melting points and high thermal stability. Due to their other unique properties, such as high chemical stability, nonflamibility, and low toxicity, ILs are being considered as greener alternatives of conventional organic solvents.[1] Recent years, therefore, have seen an increasing demand of ILs in various fields, including electochemistry,[2,3] organic synthesis,[4] material science, and in separation processes.[5,6] Moreover, their emerging ability to preserve DNA and protein for long period has added a new dimension in biotechnological research, where ILs are examined as additives for protein refolding, biomolecular crystalization, DNA extraction etc.[7,8] A major section of current research is therefore focussed on synthesising biocompatible ILs and investigating their thermophysical properties. [9-11]

Recent studies have shown that the available ILs serve better in dissolution and stability of biomolecules, when low-to-moderate concentration of water is added. Several proteins and DNA have been shown to maintain their function and native conformation in these IL/water binary mixtures.[12-17] For example, the solubility of cytochrome c (cyt. *c*) was examined in a series of ILs, containing 20 wt% water. [12,13] Among these, choline dhp/water binary mixture was found to be the best medium that could preserve the secondary structure and activity of the protein, even at high temperatures. Summers and Flowers had examined ethylammonium nitrate (EAN) as additives for protein refolding.[14] When present in concentrations upto 0.5 M, this salt effectively prevent aggregation and led to a significant increase in refolding yields. The pure liquid EAN, however, was found to denature the protein. In another study, Lange and coworkers have shown that recombinant plasminogen activator (rPA) could be refolded with increasing yields in solutions of 1-butyl-4-methyl-pyridinium-tetrafluoroborate/water.[15] Recent developments also indicated that IL/water binary mixtures are ideal solvent media for long-term DNA storage.[16,17] MacFarlane and co-workers have shown that the structural and chemical stability of DNA can be preserved up to one year in a series of choline-based ILs/water binary mixtures.[16]

It has also been demonstrated that, by selecting appropriate IL cation-anion combinations and extent of added water, properties such as density, viscosity, compressibility of ILs can be rationally modified to enable a particular application.[18-23] Jacquemin et al. have measured the densities and viscosities of several pure and water-saturated ILs by varying the IL cations and

anions. The influence of IL ion type on the thermophysical properties of both neat and IL/water binary mixtures was evident from their data.[18] Densities and viscosities of 1,1,3,3-tetramethylguanidium lactate ([TMG]L) mixed with water of different concentrations were determined by Tian et al.[19] It was found that when the mole fraction of water was lower than 0.5, the water content did not have an obvious influence on the density of [TMG]L. When the mole fraction of water was greater than 0.5, the density of the mixture decreased with further addition of water. However, viscosity of [TMG]L decreased monotonically with increased water content. Several other studies also have reported decrease in density and viscosity, with increasing water concentrations for ILs with different cation-anion combinations.[20,21] While comparing the density-viscosity data for some of the common IL/water mixtures, an interesting trend was observed. The viscosity was consistently lower for the denser IL/water solutions.[18,22,23] Notably, none of the above studies provided a detailed explanation on the observed changes in the thermophysical properties of these delicate mixtures, presumably due to the inherent limitations involved in the techniques used. *Ab-initio* quantum mechanical calculations and molecular dynamics simulations have shown tremendous potential at this end, which provide atomic level description of a complex chemical system and even can explain their anomalous behaviour, which are sometimes beyond the scope of existing experimental methods.[24-26]

In this work, we have synthesized two guanidinium cation (Fig. 1) based biocompatible ILs, tetramethylguanidinium benzoate, [TMG][BEN] and tetramethylguanidinium salicylate, [TMG][SAL] and measured their thermophysical properties, such as density (d), viscosity (η) and compressibility (κ_s) in presence of water. Results show that both the synthesized ILs are nontoxic. Results also show that [TMG][SAL]/water mixtures have higher density and partial molar volume than the [TMG][BEN]/water binary mixture, presumably due to the higher molecular weight of the [SAL] anion. However, an opposite trend was seen in viscosity and compressibility measurements, where the [TMG][SAL]/water mixtures exhibited lower viscosity and larger compressibility than the [TMG][BEN]/water mixtures. Ab initio calculations and MD simulations were performed to explain these experimental measurements and the results are presented in the subsequent sections.

2. Experimental and Computational Methods:

2.1 Synthesis and characterization of the ILs

1,1,3,3-tetramethylguanidine (＞99%, CAS No. 80-70-6, *Sigma Aldrich* Co., Ltd.) was used without further purification. Benzoic acid (≥99.9%, CAS No. 65-85-0, Rankem Laboratory Chemicals, Ltd), Salicylic acid (≥99%, CAS No. 69-72-7, Sisco Research Laboratories Pvt Ltd), and Ethanol (≥99.9%, CAS No. 64-17-5, Merck KGaA, Ltd) were all of analytical grade**.** ILs, [TMG][BEN] and [TMG][SAL] were prepared by neutralization of 1,1,3,3-tetramethylguanidine with benzoic acid and salicylic acid, respectively, according to the scheme presented in Figure S1. In our synthesis method, 100 ml ethanol and 2.30 g TMG (20.0 mmol) were loaded into a 250 ml flask in a water bath of 25^0C. Then 20.0 mmol acid (benzoic acid or salicylic acid) in 35 ml ethanol was charged into the flask under stirring. The reaction took 2 hours. The product mixture was evaporated under reduced pressure. The crude oily residue was dissolved in 100 ml ethanol, treated with active carbon, filtered, and subsequently evaporated under vacuum. The obtained ILs were characterized by differential scanning calorimetry (DSC, Perkin-Elmer DSC-7) and thermogravimetric analysis (TGA, Perkin-Elmer TGA-7). ^{1}H NMR, ^{13}C NMR spectra were recorded on a Bruker AM 500 spectrometer and are shown in Fig. S2 and S3: ^{1}H NMR (500MHz, D_2O) 2.94(s, 12 H), 7.48(m, 2 H) 7.57(m, 1 H), .7.88(m,2 H) for [TMG][BEN] and ^{1}H NMR (500MHz, D_2O) 2.87(s, 12 H), 6.93(m, 2 H) 7.45(m, 1 H), 7.81(m, 1 H) for [TMG]SAL]. HRMS were calculated for cations and anions and the results are as follow positive ion: m/z: 116 ($M+H^+$), negative ion m/z: 121 ($M-H^-$) for [TMG][BEN] and positive ion: m/z: 116 ($M+H^+$), negative ion m/z: 137 ($M-H^-$) for [TMG][SAL].

2.2 Measurements of thermophysical properties of the IL/water mixtures

All the IL/water solutions were made in freshly degassed milli-Q water and prepared on a molality basis, and whenever necessary the concentration values were converted to molarity scale using density data at 298.15. All the solutions were freshly prepared with a precision of ±0.01 mg. The samples were kept in a desiccators to avoid the atmospheric humidity. The density and speed of sound were measured with an Anton Paar (DSA 5000 M) instrument, which employs the well-known oscillating U-tube principle (for density measurement). A Lovis 2000 ME viscometer was used to measure the dynamic viscosity of the binary solutions. The temperature is controlled by a built-in Peltier thermostat. At regular intervals

of time, the densitometer was calibrated at atmospheric pressure with dry air and freshly degassed milli-Q water and the Lovis instrument was calibrated with the reference liquid. The samples were loaded into the cell and the Lovis capillary and the measurements were carried out in slow equilibration mode. The uncertainties in the measurement of density, speed of sound, and viscosity were ± 5 × 10^{-3} kg·m^{-3}, ± 0.02 m·s^{-1} and ± 0.002 mPa·s, respectively.

The Karl Fischer Titrator from Analab (Micro Aqua Cal 100) was used to measure the water content. The thermal decomposition data were obtained using TGA instrument (TA instruments Hi-Res. TGA Q500) with weighing precision of ±0.01% at a heating rate of 10°C·min^{-1} under nitrogen atmosphere in a open platinum pan. To ensure simultaneous measurement of sample temperature and heating rate control accurately and precisely, two thermocouples are positioned immediately adjacent to the sample. Curie point temperature calibration was carried out with Nickel metal. The phase transition measurements were carried out by DSC instrument (TA instruments DSC Q200) having sensitivity 0.2μW and temperature accuracy ±0.1°C. The Tzero hermatic aluminum pan is used for better resolution. Heat flow (ASTM E968) and baseline calibration were carried out with Indium metal and sapphire respectively. Scanning sequence involves freezing the IL sample to −80°C, maintaining this temperature for 20 min., and then heating the sample to 50°C with a heating rate of 2°C.min^{-1} under nitrogen atmosphere with a flow rate of 50 cm^3.min^{-1}.

2.3 *Ab initio* calculations

Ab initio calculations were performed using the Gaussian09 program.[27] Geometry optimizations, single point energy calculations, and vibrational frequency analysis were performed at the level of density functional theory (DFT) using the B3LYP/6-311++G* basis set. Various different initial configurations are considered, in which cation, anion and water molecules were placed at different locations. Optimizations of these configurations were performed without any constraints in the geometry. The lowest energy structure among all the explored geometries was designated as the optimized structure. The optimized structures represented true minima since no imaginary frequency was observed in the harmonic frequency analysis. The basis set superposition errors (BSSEs) were corrected using the counterpoise method of Boys and Bernadi.[28] The atom-centered point charges were determined *via* fits to the electrostatic potentials obtained from the calculated wave functions using the CHelpG subroutine of Gaussian09.

2.4 Modelling and simulation details

The standard molecular mechanics (MM) potential energy function of the following form was adopted to delineate the various interaction points in the IL-water binary systems.

$$E = \sum_{bond} k_r(r - r_0)^2 + \sum_{angle} k_\theta(\theta - \theta_0)^2 + \sum_{dihedrals} \frac{k_\emptyset}{2}[1 + cos(n\emptyset - \gamma)] + \sum_i \sum_{i<j} \left[\frac{A_{ij}}{r_{ij}^{12}} - \frac{B_{ij}}{r_{ij}^{6}} + \frac{q_i q_j}{4\Pi\varepsilon_0 r_{ij}}\right]$$

where, the first three expressions represent the bonded interactions: harmonic bond stretching, angle bending, and dihedral potential. The fourth term represents the nonbonded interactions that include the 12–6 Lennard–Jones (LJ) potential plus Coulomb potential. The equilibrium bond lengths r_0, angles θ_0, and dihedrals ϕ for both the cations and anions were obtained from the optimized geometries of the IL ion-pairs, as obtained from *ab-initio* calculation stated above. The atomic charges were also obtained from *ab-initio* calculation as presented above. The total charge on cation and anion was set at +1 and -1, respectively (Figs. S4, S5). With the exception of r_0, θ_0, ϕ, and q, all other potential parameters were taken directly from literature [29,30] and are listed in tables S1-S3.

Three different compositions of IL-water mixtures containing 80, 50, and 20 wt % of IL were generated with 512 IL ion pairs and a varying number of water molecules (depending upon the concentration of the binary system), and were placed in cubic simulation boxes for simulations. All the six simulations were performed at 25^0C temperature and 1 atm pressure. To enable volume variation, the simulations were performed in the NPT ensemble using the Nose–Hoover thermostat and barostat. Both the thermostat and barostat relaxation times were set to 0.5 ps. An equilibrium simulation of 5 ns was performed before a production run of 10 ns for each system. To compute the viscosity and difffusivity, all six systems were further simulated for additional 30 ns in NVT ensemble. The block averages of these properties were obtained by dividing the 30 ns trajectories into twelve windows of 2.5 ns length. For viscosity, the pressure tensor was saved at every time step. Periodic boundary conditions were employed in all directions. The calculation of long-range Coulombic forces was performed employing the full Ewald summation technique. The real space part of the Ewald sum and LJ interactions were cut off at 15 Å. All C–H bonds were held fixed by applying the SHAKE algorithm with a preset tolerance of 10^{-8}Å. All of the initial minimizations and

simulations were performed on 64 processors of IBM HPC resources at IIT Madras using the Amber 11.0 package.[31]

3. Results and Discussion

Two nontoxic tetramethylguanidinium cation based ILs, [TMG][BEN] and [TMG][SAL] are synthesized. Melting point and decomposition temperature of neat [TMG][BEN] were measured to be 110°C and 208°C, while that of neat [TMG][SAL] were 125°C and 235°C. Both the ILs were found to be completely miscible with water up to 80% wt fraction of IL. Various thermophysical properties of these binary mixtures were determined experimentally and the nature of intra- and inter-molecular interactions was investigated by *ab-initio* quantum mechanical calculations and classical molecular dynamics simulations. These results are presented here. Results for toxicological evaluation will be published subsequently.

Measured density and apparent molar volume of [TMG][SAL]/water were higher than [TMG][BEN]/water mixtures

We measured the density of the two binary mixtures for the whole concentration range of IL from 0 to 80 wt% and the results are presented in Fig. 2. It is evident from this figure that the density of both the mixtures increases with increasing concentrations of IL. However, the salicylate anion based IL systems exhibit higher density than the benzoate anion based systems, at all concentrations. The higher density of [TMG][SAL/water mixtures can be attributed to the higher molecular weight of the salicylate anion. This observation is consistent with the study of Brennecke and co-workers,[32] where the authors have seen an increase in density with increasing molecular weight of the anion for a series of 13 imidazolium-based ILs. Fig 2 also shows that, the variation in density is not uniform for the two binary mixtures. More precisely, the density of [TMG][SAL]/water mixtures exhibited a sharper decrease compared to the [TMG][BEN]/water mixtures, when more water was added. This could be due to differential interactions of water with the constituent ions in the two systems and will be discussed in the subsequent sections.

Apparent molar volume and partial molar volume are important thermodynamic quantities, which are often used to extract information about the nature of mixing of the solute to the solvent and also about the local structure of the solvent in the mixture. In this work, we

calculated the apparent molar volume, ϕ_v of [TMG][SAL] and [TMG][BEN] from the density of the aqueous solutions using the following equation:

$$\phi_V = \frac{M}{d} - \frac{(d - d_0)}{m.d.d_0}$$

where m is the molality of the IL (in mol/g), d and d_0 are the densities (in g/cc) of the solution and pure solvent (water), and M is the molar mass of IL (in gm/mole). The variation in the apparent molar volume of [TMG][SAL] and [TMG][BEN] as a function of the IL concentration is shown in Fig. 3. The graph exhibits three distinct features – (i) apparent molar volume of both [TMG]BEN] and [TMG][SAL] decreases at low concentration, (ii) apparent molar volume of [TMG]BEN] is smaller than [TMG][SAL] at all concentrations, and (iii) the initial decay of ϕ_v is more rapid for [TMG]SAL]. The initial decrease in ϕ_v might be the consequence of favourable attractive interactions between the IL ions and water molecules, which would pack the constituents more effectively to occupy less space. Smaller values of ϕ_v for [TMG]BEN] indicates that the attractive interaction of this IL with water could be stronger than that in the [TMG][SAL]/water mixtures. Besides, the vander Waals radius of the benzoate ion is smaller than the salicylate ion. The rapid decay of ϕ_v for [TMG][SAL] is presumably due to greater tendency of ion-ion association in this mixture at low concentrations. However, a more definitive explanation to these observations can not be presented at this juncture and we will resort to molecular dynamics simulation results in the next section to prove these speculations.

The limiting apparent molar volume, defined as the molar volume at infinite dilution can offer insight to unravel the solute-solvent interaction, since at infinite dilution the ions are infinitely distant from each other and are fully surrounded by the solvent molecules. Here, we obtained the limiting apparent molar volume, ϕ_v^0 for [TMG][SAL] and [TMG][BEN] by fitting the experimental ϕ_v values to the following well-known Redlich-Mayer equation[33]

$$\phi_V = \phi_V^0 + A\sqrt{C} + hC$$

here ϕ_v^0 is the limiting apparent molar volume at experimental temperature, C is the solute concentration in molarity, and A and h are the empirical parameters. We taken A = $1.868*10^{3/2}$ $(mol/cc)^{-3/2}$, as reported for aqueous 1:1 electrolytes at 298.15 K from the Debye-Huckel limiting law and has been used for many other IL/water binary solutions.[32]As the inset of Fig. 3 depicts, a least square fit to the graph of (ϕ_v - $1.868C^{1/2}$)

versus C at low concentrations gives ϕ_v^0 = 218.99 cc/mol for [TMG][SAL] and ϕ_v^0 = 203.53 cc/mol for [TMG][BEN]. A smaller value of limiting apparent molar volume of [TMG][BEN] might again suggest a better solute-solvent packing in [TMG][BEN]/water binary mixtures, even at infinite dilution.

Measured viscosity and isentropic compressibility showed an opposite trend

Viscosity is a very important thermophysical quantity that determines the suitability of an IL/water mixture as solvent for particular applications. Hence, we measured the viscosity of the binary mixtures of [TMG][BEN]/water and [TMG][SAL]/water at room temperature. Fig. 4 displays the change in viscosity of both the mixtures, as the IL concentration is increased. As one expects, the viscosity of both the solutions rises with more addition of IL. However, the increase in viscosity of the [TMG][BEN]/water mixture was found to be very sharp at high IL concentration. While the rise is just about three fold by increasing IL concentration from 70% to 80% in [TMG][SAL]/water mixture, it is nearly six fold in the [TMG][BEN]/water mixture. More importantly, the trend in the evolution of viscosity was inverse to that observed for density. The denser [TMG][SAL]-based solution exhibited lower viscosity compared to the [TMG][BEN]/water solution. Clearly, a molecular-level description of the solutions is necessary to explain these measurement data. Again, we need to rely upon the MD simulation results that can explore the microstructures of the solutions, simulated at experimental conditions.

We also determined the isentropic compressibility, κ_s (Pa^{-1}) of both the solutions from the measured sound velocity and density data, using Laplace–Newton's equation:

$$\kappa_s = \frac{1}{u^2 d}$$

where u (m/s) is the sound velocity of the solution. The isentropic compressibility values are plotted as a function of molality of the ILs in Fig. 5. This figure clearly shows that the compressibility of IL/water binary mixtures decreases with the increase of IL concentration, as one would expect. However, the decrease is not uniform - compressibility decreases very rapidly up to the IL concentration of 50%, but then it declines slowly. More interestingly, the [TMG][SAL]/water binary mixtures exhibited to be more compressible than the [TMG][BEN]/water mixtures at all concentrations. This is again in direct contrast with the density data. In principle, the denser [TMG][SAL] solution should have been less

compressible due to higher mass-per-volume. At this point, we can only speculate that the interactions among the constituent IL ions and their interactions with water are weaker in [TMG][SAL]/water binary mixture compared to the other mixture. Thus, a deeper understanding of the structure and nature of interactions between the constituents is warranted.

***Ab initio* calculations show the existence of [SAL] as isolated ions**

Electronic structure calculation is a very important tool in describing the lowest-energy structure and inter-atomic interaction of a substance in isolated state. Hence, we performed *ab initio* quantum mechanical calculations on the salicylate and benzoate anions and also on the ion pairs - [TMG]+[SAL] and [TMG]+[BEN] to determine their optimized structures. Fig. 6a depicts that the benzoate anion is planar with both the carboxylate oxygens carrying the same amount of negative charge due to structural resonance. The optimized structure of salicylate shows even a more unique character, where both the carboxylate and hydroxy groups were found to lie on the same plane of the phenyl ring and form an intra-molecular H-bonding (O-H distance 1.45Å, ∠O-H-O = 153.17^{o}). It is to be emphasized here that a set of other initial structures of salicylate anion, where the –OH group was kept pointing away from the carboxylate group and carboxylate group kept out of plane, converged either to the same configuration as in Fig. 6b or to a higher energy structure. Our finding is strongly supported by the UV-Vis and fluorescence measurements of Friedrich et al., where the authors have noted a intramolecularly H-bonded structure as the major tautomer in the aqueous solution of sodium salicylate.[34]

We also optimized the structures of the IL ion pairs and the results are shown in Fig. 6c,d. In this most stable configuration of the ion pairs, the guanidinium central C and the adjoining three N atoms were found to constitute a plane and the anion was situated in a nearly perpendicular orientation to this plane. To optimize the interactions, the anion carboxylate pointed itself toward the cation and one of the carboxylate oxygen formed a strong H-bond with the hydrogens of the cation NH_2 group, while the other oxygen remained in close contact with the H atoms of NMe moieties. The COO-NH_2 H-bond was so strong that it twists the NH_2 group and pushes both NH_2 hydrogen out of the guanidinum plane. We note that this optimized structure is consistent with the previously reported structure of tetramethylguanidinium-lactate and similar IL ion pairs.[35] It is worth

mentioning here that, we have performed calculations on 33 different initial configurations for each of [TMG][SAL] and [TMG][BEN] in the search for the lowest energy configurations. Fig. 6 represents the best structure among these trials. To get an understanding on the extent of interactions of the salicylate and benzoate anion with the cation, we then calculated the single point energy of these optimized ion pairs. The respective calculated energies of -83.19 kcal/mol and -90.11 kcal/mol suggest a weaker interaction of [SAL] with [TMG], presumably due to its intramolecular H-bonding and less tendency for inter-molecular interactions.

In the IL/water binary mixtures, the salicylate and benzoate anions will also involve in interactions with water. Hence, we optimized the anion-water structures and evaluated their strength of interactions. As Fig. 7 shows, both the anions form multiple H-bonds with water. However, the interaction appears to be stronger between benzoate-water as exemplified by greater energy (-18.11 kcal/mol vs. -15.98 kcal/mol). In bulk solutions, since one anion can be surrounded by many other water molecules, we have also computed the interactions of anions with two and three water molecules. Subsequently, we have checked the interactions of IL ion pairs with water in the lowest energy structures. As the results from Figs. 7 and S6 consistently show, benzoate anion and [TMG][BEN] interact with water more profoundly than the salicylate or [TMG][SAL]. The relatively large ΔE values, as included in Fig. 7 and S6, indicate that this interaction not only involves the H-bonding, but also has a significant contribution from electrostatics. Nevertheless, the result clearly signifies the propensity for the salicylate anion to remain in a more discrete state than the benzoate anion, primarily due to its intramolecular H-bonding capacity.

MD simulations showed extended H-bonding in [TMG][BEN]/water mixtures

Even though a good atomic-level description of intra- and inter-molecular interactions among the constituents in the IL/water binary mixtures was obtained from the *ab initio* calculations, the study represents only the gas phase behaviour. Hence, we performed all-atom molecular dynamics simulations to examine the behaviour of the systems in liquid phase. For each [TMG][SAL] and [TMG][BEN], we simulated three IL/water systems that represent the dense (80 wt% IL), moderately dense (50 wt% IL), and dilute (20 wt% IL) solutions of IL/water. Thus, a total of six simulations was performed in this study. First, to verify the correctness of the simulation parameters and the protocol, we computed the density of the

solutions and compared with the experimentally measured values. Table 1 lists the experimental and simulated density of all the six systems. As the table indicates, the simulated densities are in very good agreement with the experimental results.

We also calculated the viscosity of the IL/water solutions at 298K using the Green-Kubo relation[36]:

$$\eta(t) = \frac{V}{10K_BT}\int_0^t \langle Tr[\tilde{P}(t'')\tilde{P}(t'+t'')]\rangle\, dt'$$

where V is the volume of the system and $\tilde{P}$ is the symmetric traceless component of the pressure tensor. Equilibrium viscosity values were obtained from the converged values of the running integral of the pressure tensor time autocorrelation function (shown in Fig. S8) and are tabulated in Table 2. As Table 2 indicates, the trend of the calculated viscosity values matches very well with experiment, with [TMG][BEN]-based solutions showing higher viscosity at all concentrations. This correct capturing of the divergent trend in density *versus* viscosity of the two IL solutions as seen in experiments, gives us confidence to utilize the MD simulation data to explain the experimental observations at atomic detail. However, it is worth mentioning here that the calculated viscosity for the 80:20 IL/water solutions shows an overestimation by a factor of about 3.5. This is consistent with prior MD simulation studies of neat ILs that reported a similar or higher fold of overestimated viscosity, using the traditional force fields comprising full unit charge on IL ions.[37-39] Interestingly, as the solution becomes more dilute the deviation from experimental value decreases (Table 2), which can be attributed to the screening of IL ion charges by added water.

In MD simulations, the structure of a solution is best described by calculating the radial distribution functions of its constituents. Radial distribution functions (RDFs) essentially describe the probability of finding one component around another in the solution. Thus, to describe the liquid structure of our binary IL/water mixtures, we calculated RDFs for the pairs of water-anion, water-cation, cation-anion etc. Fig. 8 depicts the distribution of water around the IL anions in both [TMG][SAL] and TMG][BEN] solutions. We would like to emphasize here that, to determine the primary site of interaction of water with the anions, we examined all possible sites and found carboxylate oxygens to be the most effective sites of the anions for interaction with water oxygen. Hence, site-site RDFs for water-anion were computed for O_w-O_{COO} *i.e.,* water oxygen-carboxylate oxygen. Sharp peak in Fig. 8 indicates

strong and site-specific interactions between water and the anions in both the systems. Moreover, the presence of the first minima at < 3.5 Å is indicative of the existence of hydrogen bonds between water and carboxylate group (geometric definition of H-bond[40]). Also, the peak intensity rises in dense systems, implying better anion-water association as water content increases in the system. However, the most noteworthy feature of Fig. 8 is that, irrespective of the IL concentration in the systems, the peak intensity is always higher for [TMG][BEN] system. This clearly indicates a stronger interaction between [BEN] and water than [SAL] and water, as was also suggested by *ab initio* calculations.

We also checked the distribution of water around [TMG] cation in both set of systems. A similar trend is observed for cation-water RDFs. However, the peak intensities were found to be much smaller than the anion-water, implying a more dominant role of the anion in the interaction with water. This is consistent with prior studies, which have shown that IL anions play the primary role in solvation and gas solubility.[41-44] The distribution was also found to be broader compared to the anion-water distribution, implying the presence of a weaker site-specific interaction of water with [TMG], presumably due to the bulky $–N(Me)_2$ groups in [TMG] that make water access to $–NH_2$ group difficult. The most striking feature of Fig. 9, however, is that, in spite of the cation being common in both the systems, it shows a higher interaction with water in [TMG][BEN] systems, particularly at high IL concentration. This is due to the influence of the anion, where the strongly interacting benzoate anion induces [TMG] for better interaction with water. This again reiterates the primary influence of IL anion in solvation.

Thus, both *ab initio* and MD simulation results have revealed the existence of strong IL ion-water interaction in our studied systems and this explains the experimentally observed decreased apparent molar volume at low concentration, as shown in Fig. 3. The stronger [TMG][BEN]-water interaction also could explain the measured lower molar volume of [TMG][BEN]/water compared to the [TMG][SAL]/water mixtures. To explain the sharper decrease in ϕ_v of [TMG][SAL]-based system at lower concentrations, we resort to cation-anion distribution in these systems, which are shown in Fig. 10. As this figure shows, at low concentrations, the cation-anion association in [TMG][SAL] is greater than [TMG][BEN]. Both the anion and cation in [TMG][SAL] systems have weaker interaction with water. Hence, at low concentration they prefer to stay together. On the other hand, the more efficient

H-bond making capacity of both [BEN] and [TMG] in [TMG][BEN] make this IL better hydrated. The poorly hydrated [TMG]-[SAL] ion pair breaks the local solvent network in large extent, which manifests in sharp decrease in ϕ_v values. Fig. S7 presents such a distribution of solvent molecules around a representative IL ion pair from MD simulations. The closely associated cation-anion pair of [TMG] and [SAL] disrupts local water-water H-bonding and orient them in a fashion very similar to the hydrophobic solutes, such as benzene that produces water cage surrounding it in water.[45] This is not surprising, as both the phenyl group and intramolecularly H-bonded carboxylate and hydroxyl substituent make [SAL] weakly hydrophilic.

To explain the anomalous trend in experimental viscosity and compressibility data, we performed H-bond analysis on the MD trajectories and also computed the translation diffusion coefficients of the constituents of IL solutions. Fig. 11a compares the average number of H-bonds that [SAL] and [BEN] ions make with water in the respective solutions. The geometric definition of H-bond is used to count the number of H-bonds, where a H-bond is considered to be formed if a radial distance of < 3.5 Å between the donor and acceptor atoms and a donor-H-acceptor angle > 135^o is present.[40] As Fig. 11a demonstrates, benzoate anion always forms larger number of H-bonds with water than the salicylate anion. The [TMG] cation of [TMG][BEN] also shows a higher cation-water H-bonding capacity than the [TMG] in [TMG][SAL] (data not shown). As a corollary, the water-water H-bonding shows a slight rise in [TMG][SAL]/water mixture than the benzoate-based mixture, as shown in Fig. 11b. To visualize this distribution more directly, we have presented the distributions of the constituents of both the mixtures in Fig. 12 from MD simulation data. The extended H-bonding network in benzoate anion system is evident. This makes the [TMG][BEN]/water solutions better packed. In contrast, lesser hydrophilicity of the salicylate anion leaves [TMG][SAL] as discrete ion-pairs with poor IL-water packing. These findings from H-bond analysis tempted us to conclude that the presence of the extended H-bonding network comprised of [BEN]-water, [TMG]-water, and water-water in [TMG][BEN]/water makes this solution very viscous and less compressible. On the other hand, the weaker IL-water interaction in [TMG][SAL/]water system leaves [TMG][SAL] as discrete ion-pairs with random distribution of water clusters in the solution.

However, recent studies have pointed out that increased hydrogen bonding in ILs, particularly those of imidazolium-based does not "always" lead to higher viscosity.[46,47] Hence, we have computed translational diffusivity to better correlate the extent of H-bonding with the dynamical properties of the solutions. The self-diffusivity, D was calculated by using the Einstein's relation:

$$D = \frac{1}{6} \lim_{t \to \infty} \frac{d}{dt} \langle \Delta r(t)^2 \rangle$$

where the brackets denote an ensemble average and the quantity in brackets is the mean square displacement of a given component in solution at time t. The calculated values in Table 3 clearly indicate that both IL ions and water in [TMG][BEN]/water solutions diffuse slower than those in the [TMG][SAL]/water solutions. The slower diffusion of [TMG][BEN] solution at all concentrations correlates very well with its higher viscosity, which again can be ascribed to greater H-bonding and inter-particle interactions in this solution. It is possible that the loss of entropy that overwhelmed the effects due to loss in hydrogen bonding in imidazolium ILs has minimal influence on our ILs of interest, since none of our IL ions has a long alkyl chain or large asymmetry in structure.

4. CONCLUSIONS

In this work, we report the synthesis and characterization of two novel tetramethylguanidinium cation-based ionic liquids, [TMG][SAL] and [TMG][BEN]. Both the synthesized ILs were nontoxic. A number of thermophysical properties of the binary aqueous solutions of these ILs, such as density, viscosity, compressibility were measured. To the best of our knowledge, this is the first report of the synthesis and characterization of [TMG][SAL] and its binary aqueous mixture. Results show that [TMG][SAL]/water mixtures have higher denisty and apparent molar volume than the [TMG][BEN]/water binary mixture, presumably due to the higher molecular weight of the [SAL] anion. However, an opposite trend was observed in measured viscolsiy and compressibility data, where the more dense [TMG][SAL]/water mixtures exhibited lower viscosity and larger compressibility than the [TMG][BEN]/water mixtures. Interestingly, a similar divergent trend in density *versus* viscosity was reported for many other IL/water mixtures (refs. 18, 22, 23). However, no attempt has been made to understand the molecular basis of such interesting observations.

Here we have employed *ab initio* calculations and MD simulations to explain these observations from differential molecular interactions and ionic hydrations in our two newly-prepared tetramethylguanidinium based IL/water mixtures. A distinctly different solvation process was seen to occur in the two studied solutions. While the closely associated cation-anion pairs disrupt the local water-water H-bonding network in [TMG][SAL]/water mixtures, the constituent ions in [TMG][BEN]-based solution incorporate very well into the water structure. This is due to the intramolecular H-bonding in salicylate anions that makes it weakly interacting with water. On the other hand, the unhindered H-bond making capacity of the benzoate anions facilitates a continuous H-bonded network, comprising of [BEN]-water, [TMG]-water, water-water in [TMG][BEN]/water solution. This makes the latter systems more viscous and stiffer. The study paves way for testing this series of ILs in biomolecular dissolution and stability.

SUPPORTING INFORMATION

Following Supporting Figures and Tables are provided: Figures S1 – S8, Tables S1-S3.

ACKNOWLEDGEMENTS

We are very thankful to Mr. Anirban Mondal and Prof. Sundaram Balasubramanian for their help in viscosity calculation. Computer resource of Computer Centre, IIT Madras is also gratefully acknowledged.

REFERENCES

1. N. V Plechkova and K. R. Seddon, *Chem. Soc. Rev.,* 2008, **37**, 123–150.
2. D. R. MacFarlane, J. M. Pringle, P. C. Howlett and M. Forsyth, *Phys. Chem. Chem. Phys.,* 2010, **12**, 1659–1669.
3. M. Yoshizawa, A. Narita and H. Ohno*, Aust. J. Chem.,* 2004, **57**, 139–144.
4. T. WELTON, *Chem. Rev*., 1999, **99,** 2071−2083.
5. L. C. Branco, J. G. Crespo and C. A. M. Afonso, *Angew. Chemie - Int. Ed.,* 2002, **41**, 2771–2773.
6. M. L. Dietz, *Sep. Sci. Technol.,* 2006, **41**, 2047–2063.
7. N. Byrne, L.-M.Wang, J.-P. Belieres and C. A. Angell, *Chem. Commun.* 2007, 2714–2716.
8. J. H. Wang, D. H. Cheng, X. W. Chen, Z. Du and Z. L. Fang, *Anal. Chem.*, 2007, **79**, 620–625.
9. X. D. Hou, Q. P. Liu, T. J. Smith, N. Li and M. H. Zong, *PLoS One,* 2013, **8**.
10. R. F. M. Frade, A. A. Rosatella, C. S. Marques, L. C. Branco, P. S. Kulkarni, N. M. M. Mateus, C. A. M. Afonso and C. M. M. Duarte, *Green Chem.,* 2009, **11**, 1660.
11. D. J. Tao, Z. Cheng, F. F. Chen, Z. M. Li, N. Hu and X. S. Chen, *J. Chem. Eng. Data,* 2013, **58**, 1542–1548.
12. K. Fujita, M. Forsyth, D. R. MacFarlane, R. W. Reid and G. D. Elliott, *Biotechnol. Bioeng.,* 2006, **94,** 1209–1213.
13. K. Fujita, D. R. MacFarlene, M. Forsyth, M. Yoshizawa-Fujita, K. Murata, N. Nakamura and H. Ohno, *Biomacromolecules*, 2007, **8**, 2080–2086.
14. C. A. Summers and R. A. Flowers, *Protein Sci.,* 2000, **9**, 2001–2008.
15. C. Lange, G. Patil and R. Rudolph, *Protein Sci.,* 2005, **14**, 2693–2701.R.
16. Vijayaraghavan, A. Izgorodin, V. Ganesh, M. Surianarayanan, D. R. MacFarlane, *Angew. Chem., Int. Ed.* 2010, **49,** 1631−1633.
17. Chandran, D. Ghoshdastidar and S. Senapati, *J. Am. Chem. Soc.,* 2012, **134,** 20330–20339.
18. J. Jacquemin, P. Husson, A. A. H. Padua and V. Majer, *Green Chem.,* 2006, **8,** 172.

19. S. N. Tian, S. Ren, Y. Hou, W. Wu, and W. Peng, *J. Chem. Eng. Data* 2013, **58**, 1885−1892..

20. C. A. Hall, K. A. Le, C. Rudaz, A. Radhi, C. S. Lovell, R. A. Damion, T. Budtova and M. E. Ries, *J. Phys. Chem. B*, 2012, **116**, 12810–12818.

21. W. Guan, X. X. Ma, L. Li, J. Tong, D. W. Fang and J. Z. Yang, *J. Phys. Chem. B,* 2011, **115**, 12915–12920.

22. H. Rodríguez and J. Brennecke, *J. Chem. Eng. Data*, 2006, **51**,2145–2155.

23. B. Mokhtarani, A. Sharifi, H. R. Mortaheb, M. Mirzaei, M. Mafi and F. Sadeghian, *J. Chem. Thermodyn.,* 2009, **41**, 323–329.

24. D.Ghoshdastidar and S. Senapati, *J.Phys.Chem. B,* DOI:10.1021/acs.jpcb.5b00433.

25. A. Mondal and S. Balasubramanian, *J. Phys. Chem. B*, 2014, **118,** 3409–3422.

26. A.Mondal and S.Balasubramanian, *J.Phys.Chem.B,*DOI: 10.1021/acs.jpcb.5b02272

27. M. J. Frisch, et al *Gaussian 09, Revis.* A.02, 2009.

28. S. F. Boys, F. Bernardi, *Mol. Phys.* 1970, **19**, 553–556.

29. S. Aparicio and M. Atilhan, *J. Phys. Chem. B*, 2012, **116**, 9171–9185.

30. Chandran, K. Prakash and S. Senapati, *Chem. Phys.* 2010, **374**, 46–54.

31. D. A. Case, T. A. Darden, I. I. I. Cheatham T.E., C. L. Simmerling, J. Wang, R. E. Duke, R. Luo, R. C. Walker, W. Zhang, K. M. Merz, et al. *AMBER 11, Univ. California, San Fr.,* 2010

32. P. Fredlake, J. M. Crosthwaite, D. G. Hert, S. N. V. K. Aki and J. F. Brennecke, *J. Chem. Eng. Data,* 2004, **49**, 954–964.

33. H. Dagade, K. R. Madkar, S. P. Shinde and S. S. Barge, *J. Phys. Chem. B*, 2013, **117**, 1031–1043.

34. M. Friedrich, Z. Wang, A. G. Joly, K. A. Peterson and P. R. Callis, *J. Phys. Chem. A,* 1999, **103**, 9644–9653.

35. G. Yu and S. Zhang, *Fluid Phase Equilib.,* 2007, **255**, 86–92.

36. P. J. Daivis and D. J. Evans, *J. Chem. Phys.,* 1994, **100**, 541.

37. M. Chen, R. Pendrill, G. Widmalm, J.W. Brady, and J. Wohlert, *J. Chem. Theory Comput.* 2014, **10,** 4465−4479

38. T. V.-O. Nguyen, C. Houriez and B. Rousseau, *Phys. Chem. Chem. Phys.*, 2010, **12**, 930–936.

39. V. V. Chaban, I. V. Voroshylova and O. N. Kalugin, *Phys. Chem. Chem. Phys.*, 2011, **13**, 7910.

40. M.Brehm, H.Weber, A.S. Pensado, A. Starkb and B. Kirchner, *Phys. Chem. Chem. Phys.,* 2012, **14,** 5030–5044

41. G. Yu and X. Chen*, J. Phys. Chem. B,* 2011, **115,** 3466–3477.

42. B. R. Prasad and S. Senapati, *J. Phys. Chem. B*, 2009, **113**, 4739–4743.

43. Chandran, K. Prakash and S. Senapati, *J. Am. Chem. Soc.,* 2010, **132,** 12511–12516.

44. L. I. N. Tomé, M. Domínguez-Pérez, A. F. M. Cláudio, M. G. Freire, I. M. Marrucho, O. C. Oscar Cabeza and J. A. P. Coutinho, *J. Phys. Chem. B*, 2009, **113**, 13971–13979

45. M. Allesch, E. Schwegler, W. G. Galli, *J. Phys. Chem. B* 2007, **111**, 1081–1089.

46. P. A. Hunt, *J. Phys. Chem. B,* 2007**, 111,** 4844-4853.

47. K. Fumino, A. Wulf, and R. Ludwig, *Angew. Chem. Int. Ed.* 2008, **47,** 8731 –8734.

48. M.W. Mahoney and W. L. Jorgensen, J. Chem. Phys. , 2001,**114**, 363.

Table 1. Comparison of experimental and simulated densities of the IL/Water mixtures.

Composition (wt %)	Experimental density (g /cc)	Density from MD Simulations (g /cc)
80 % [TMG][SAL] + 20 % water	1.1411	1.2180
50 % [TMG][SAL] + 50 % water	1.0857	1.1230
20 % [TMG][SAL] + 80 % water	1.0320	1.0341
80 % [TMG][BEN] + 20 % water	1.1205	1.1910
50 % [TMG][BEN] + 50 % water	1.0758	1.1100
20 % [TMG][BEN] + 80 % water	1.0266	1.0302

Table 2. Comparison of experimental and simulated viscosities of the IL/Water mixtures.

Composition (wt %)	Experimental viscosity (mPa.s)	Viscosity from MD Simulations (mPa.s)
80 % [TMG][SAL] + 20 % water	63.52	225.04 ± 18.50
50 % [TMG][SAL] + 50 % water	5.31	3.85 ± 0.50
20 % [TMG][SAL] + 80 % water	1.75	0.66 ± 0.03
80 % [TMG][BEN] + 20 % water	182.84	627.40 ± 21.50
50 % [TMG][BEN] + 50 % water	6.91	4.66 ± 0.56
20 % [TMG][BEN] + 80 % water	2.00	0.84 ± 0.04

Table 3. Translational diffusion coefficients (10^{-9} m^2/s) of the constituent IL ions and water in the IL/water binary mixtures at 298K.

Composition (wt %)	D_{cation}	D_{anion}	$^{a}D_{water}$
80 % [TMG][BEN] + 20 % water	0.003 ± 0.0001	0.002 ± 0.0002	0.017 ± 0.0003
50 % [TMG][BEN] + 50 % water	0.152 ± 0.0034	0.122 ± 0.0015	0.876 ± 0.0081
20 % [TMG][BEN] + 80 % water	0.909 ± 0.0267	0.743 ± 0.0061	3.333 ± 0.0116
80 % [TMG][SAL] + 20 % water	0.006 ± 0.0003	0.005 ± 0.0001	0.035 ± 0.0010
50 % [TMG][SAL] + 50 % water	0.216 ± 0.0008	0.170 ± 0.0016	1.038 ± 0.0093
20 % [TMG][SAL] + 80 % water	1.017 ± 0.0083	0.830 ± 0.0033	3.536 ± 0.0041

[a]Reported diffusivity of TIP3P water is 5.06 X 10^{-9} m^2/s.[48]

FIGURE LEGENDS

Figure 1. Molecular structures of (a) 1,1,3,3-tetramethylguanidinium cation, (b) benzoate anion and (c) salicylate anion.

Figure 2. Variation of density of the binary mixtures of [TMG][BEN]/water (circle) and [TMG][SAL]/water (square) with the concentration of IL at 298.15 K. Experimental points are connected to aid the eye.

Figure 3. Variation of apparent molar volume of [TMG][BEN] (black) and [TMG][SAL] (red) in the IL/water binary mixtures with IL concentration. Inset shows the fitting of the molar volume at dilute concentrations to the RM equation.

Figure 4. Variation of viscosity of the IL/water binary mixtures with the concentration of IL at 298.15 K. Color scheme is similar to Fig.2.

Figure 5. Variation of the isentropic compressibility of the IL/water binary mixtures with the concentration of IL at 298.15 K. Color scheme is similar to Fig.2.

Figure 6. Minimum energy structures of (a) [BEN] anion, (b) [SAL] anion, (c) [TMG][BEN] ion pair, and (d) [TMG][SAL] ion pair, obtained from *ab-initio* quantum mechanical calculations. The dotted lines represent the H-bonding interactions and the corresponding distance values are included. The distance between carboxylate oxygens (O1 and O2) and cation central carbon (C1) are shown, which signify the presence of electrostatic interactions between the ions. Interaction energies (ΔE) are obtained by subtracting the energies of the individual optimized structures of the ions from the energy of the optimized ion-pair structure. All distance are in Å and energies in kcal/mol.

Figure 7. Minimum energy structures of (a) [BEN] anion + water, (b) [SAL] anion + water, (c) [TMG][BEN] + water, (d) [TMG][SAL] + water. All other details are similar to Fig.5.

Figure 8. Distribution of water around the IL anions in the IL/water binary mixtures, as obtained from liquid phase simulations: (a) 80% IL+20% water solution, (b) 50% IL+ 50% water solution and (c) 20% IL+80% water solution. Site-site RDFs are drawn for O_w–O_{coo}. Color scheme: black for [TMG][BEN], red for [TMG][SAL].

Figure 9. Distribution of water around the IL cations in the IL/water binary mixtures, as obtained from liquid phase simulations: (a) 80% IL+20% water solution, (b) 50% IL+ 50% water solution and (c) 20% IL+80% water solution. Site-site RDFs are drawn for O_w–N_{TMG}. Color scheme is similar to Fig.7.

Figure 10. Distribution of IL anions around the IL cations in the IL/water binary mixtures, as obtained from liquid phase simulations: (a) 80% IL+20% water solution, (b) 50% IL+ 50% water solution and (c) 20% IL+80% water solution. Site-site RDFs are drawn for O_{coo}–N_{TMG}. Color scheme is similar to Fig7.

Figure 11. Hydrogen bond analysis depicting the average number of H-bonds between (a) anion and water, (b) water and water. Results are shown for all the three IL/water compositions and for both [TMG][BEN] (black) and [TMG][SAL] (red). Error bars are included.

Figure 12. Spatial arrangements of the constituents of (a) [TMG][BEN]/water and (b) [TMG][SAL]/water mixtures from MD simulations. Snapshots are obtained from the time-averaged structures of the 50:50 IL/water mixtures. Color scheme: red for oxygen, blue for nitrogen, white for hydrogen. For clarity, the hydrogens of IL cation and anions are omitted. The dotted lines represent the H-bonds.

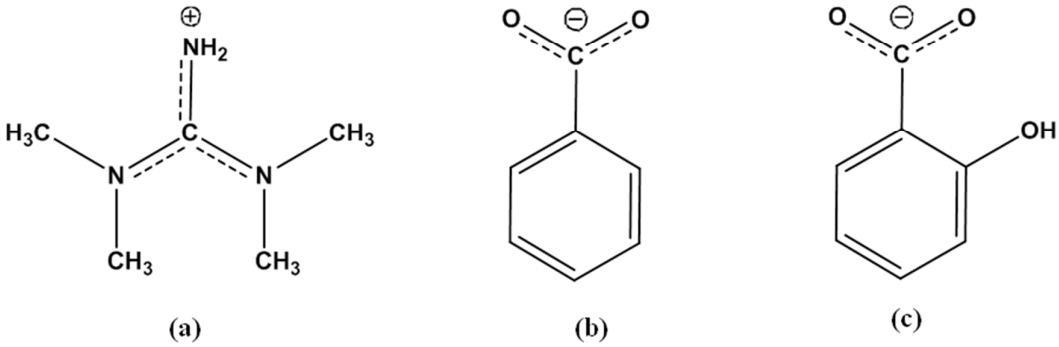

(a) (b) (c)

Figure. 1

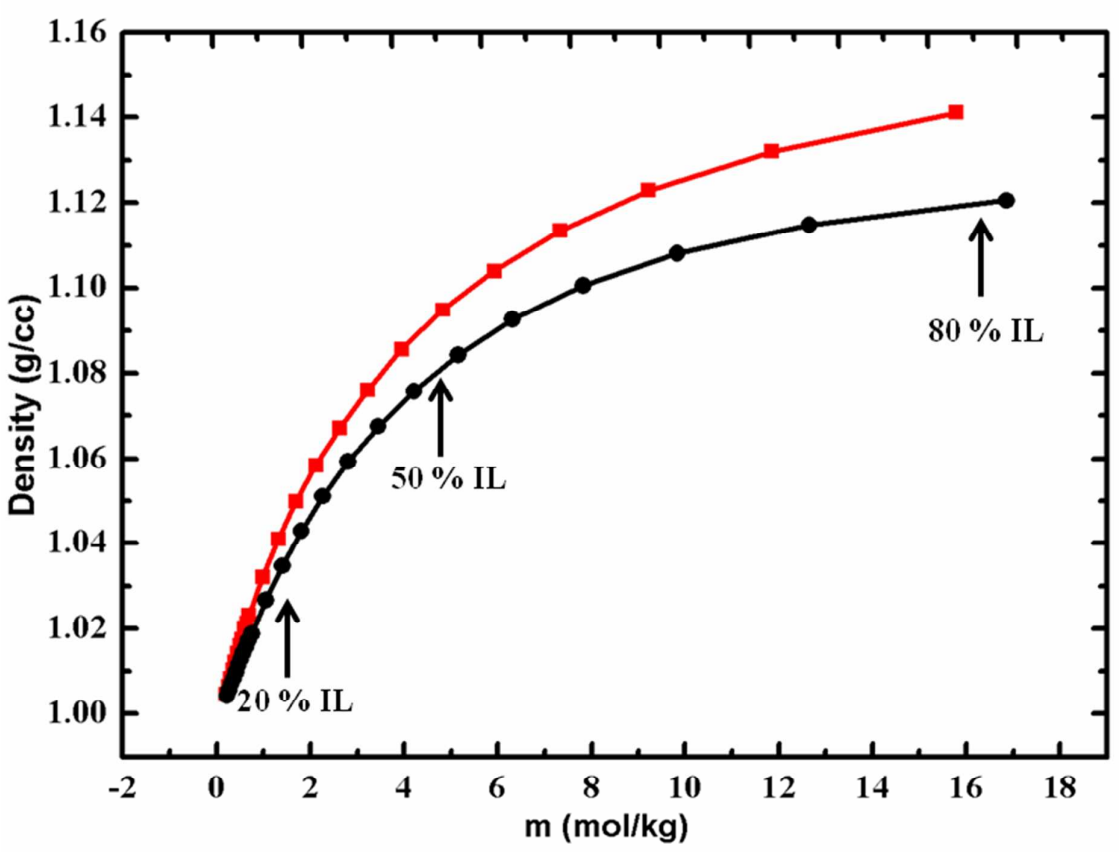

Figure 2.

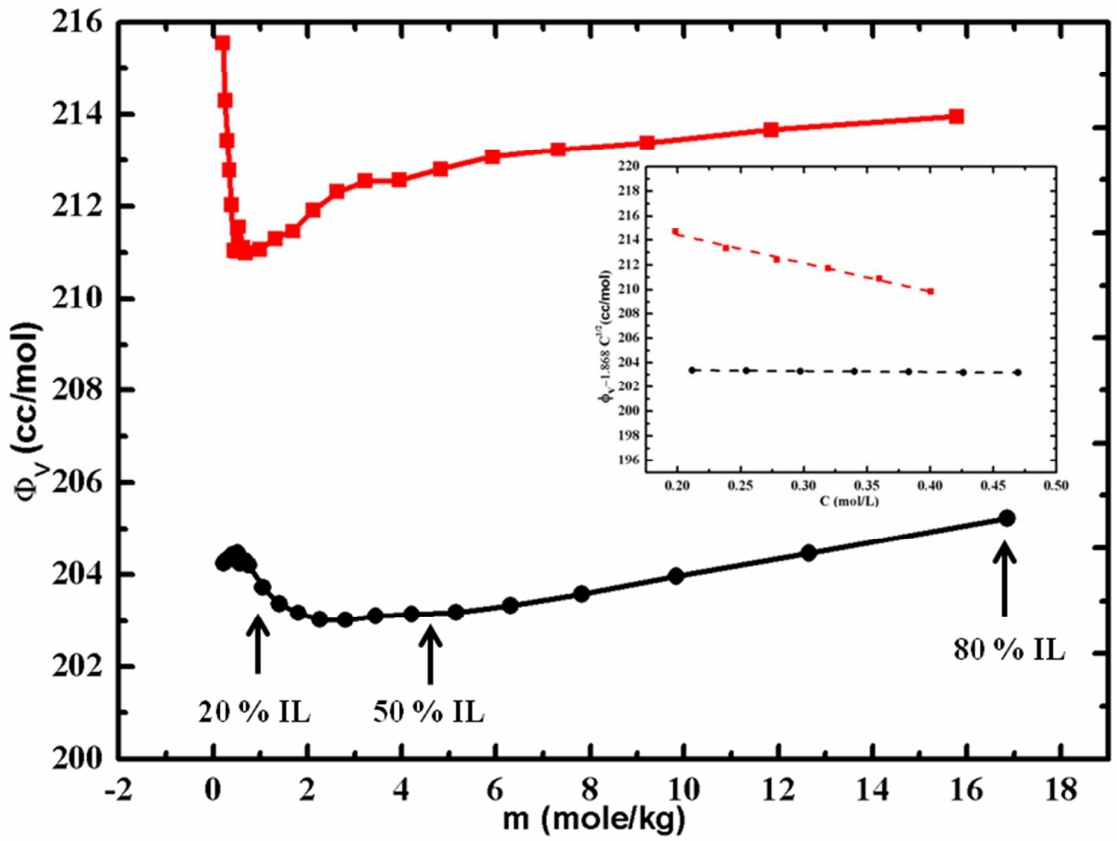

Figure 3.

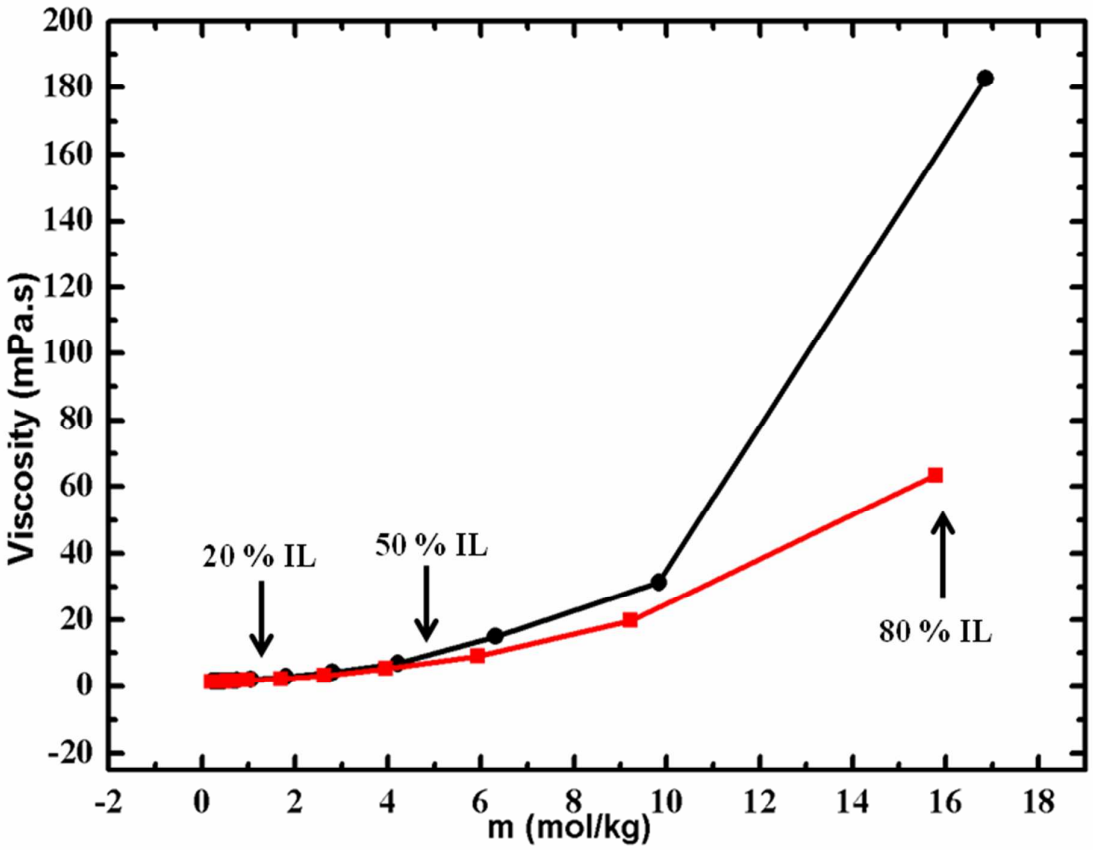

Figure 4.

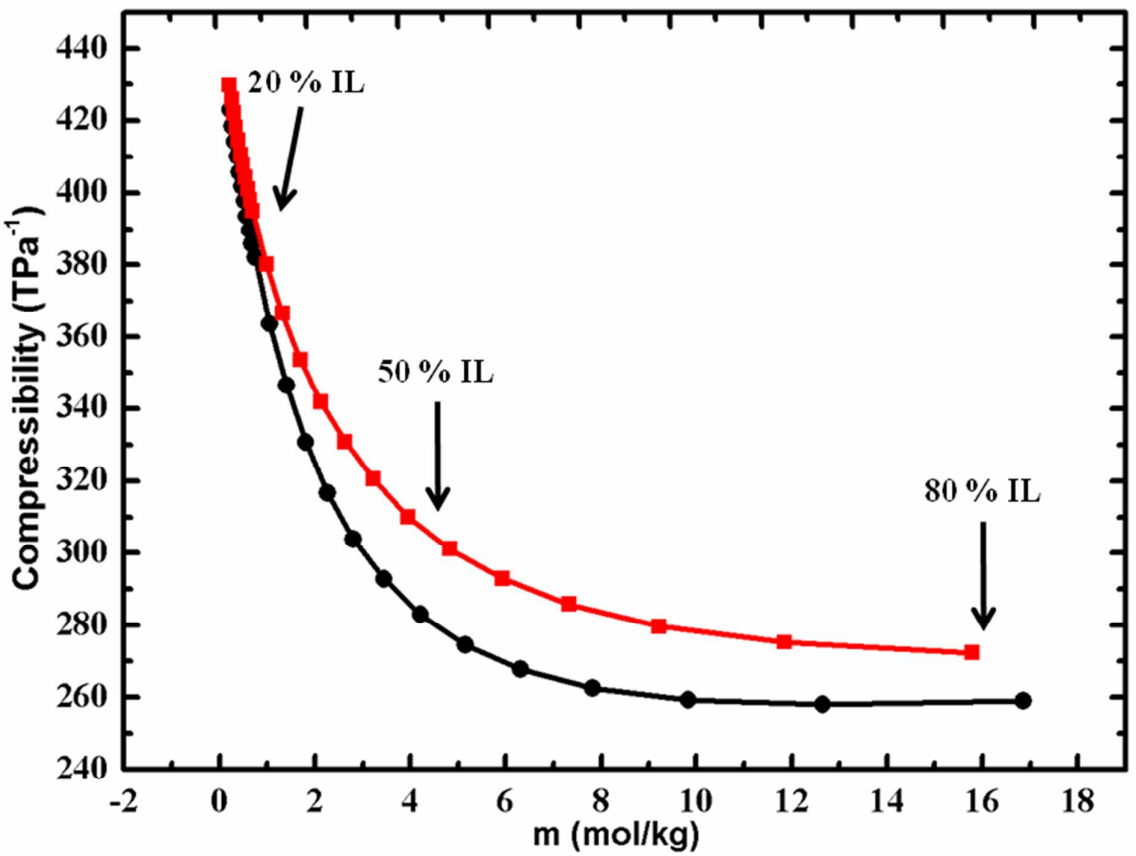

Figure 5.

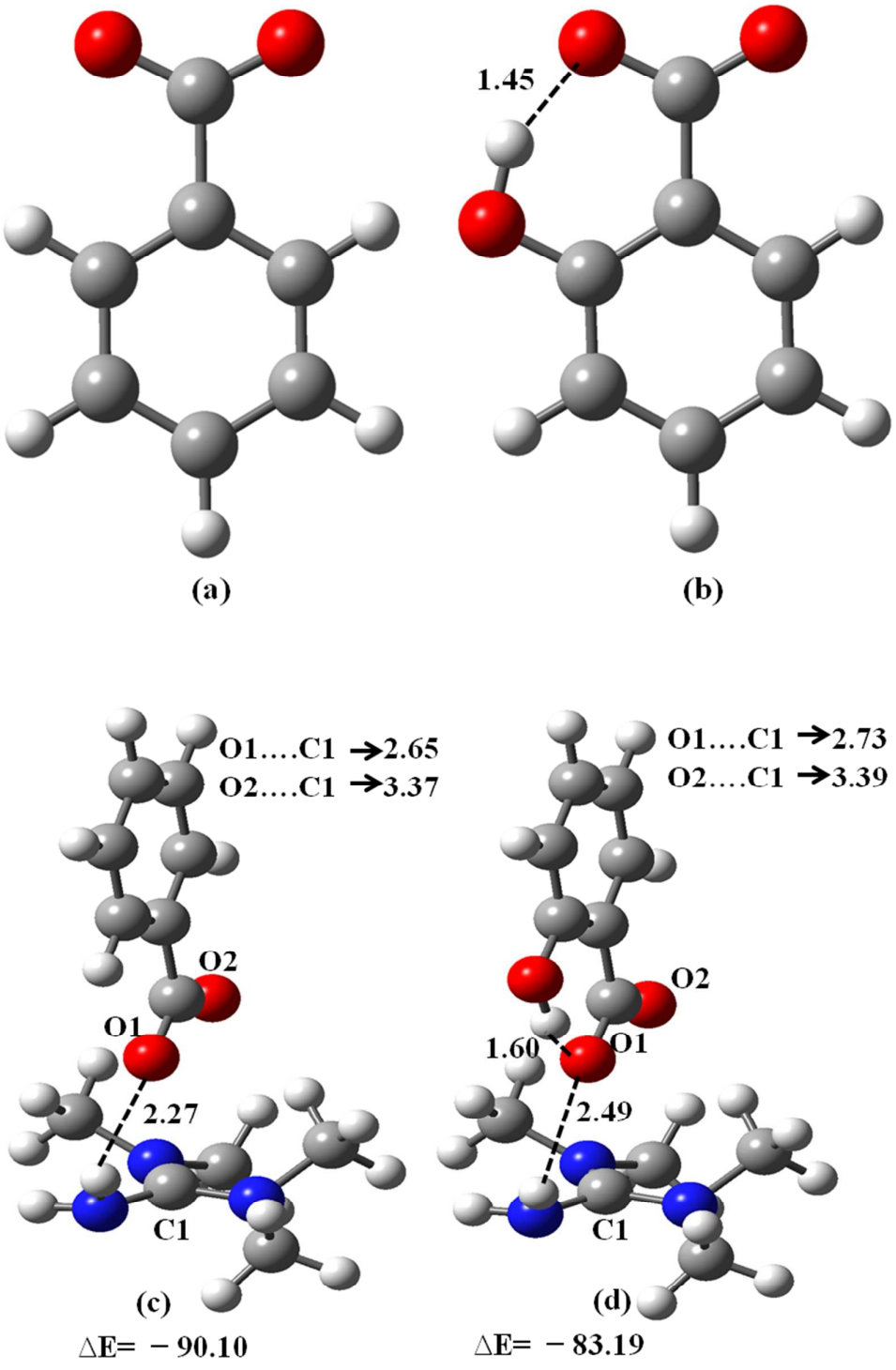

Figure 6.

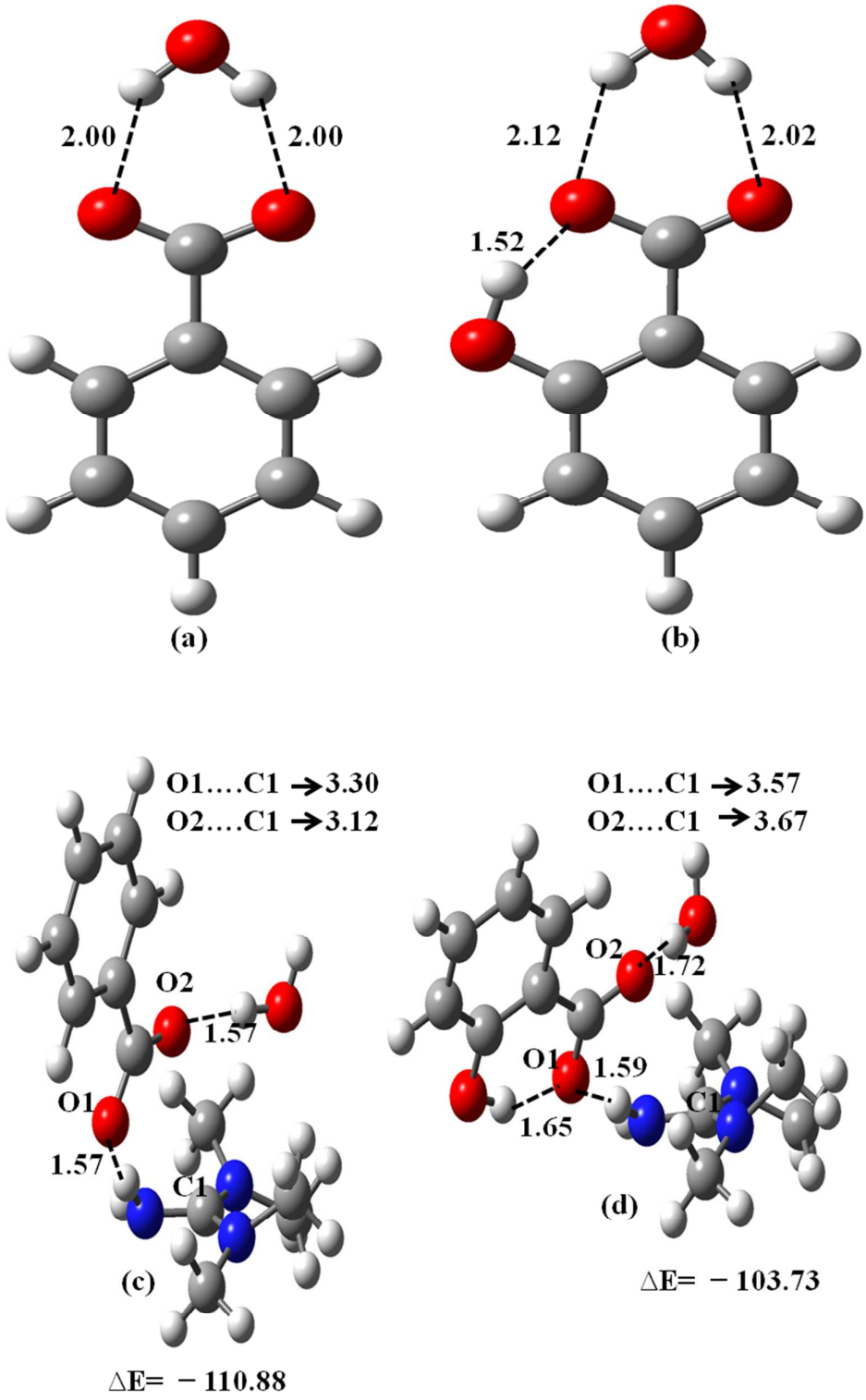

Figure 7.

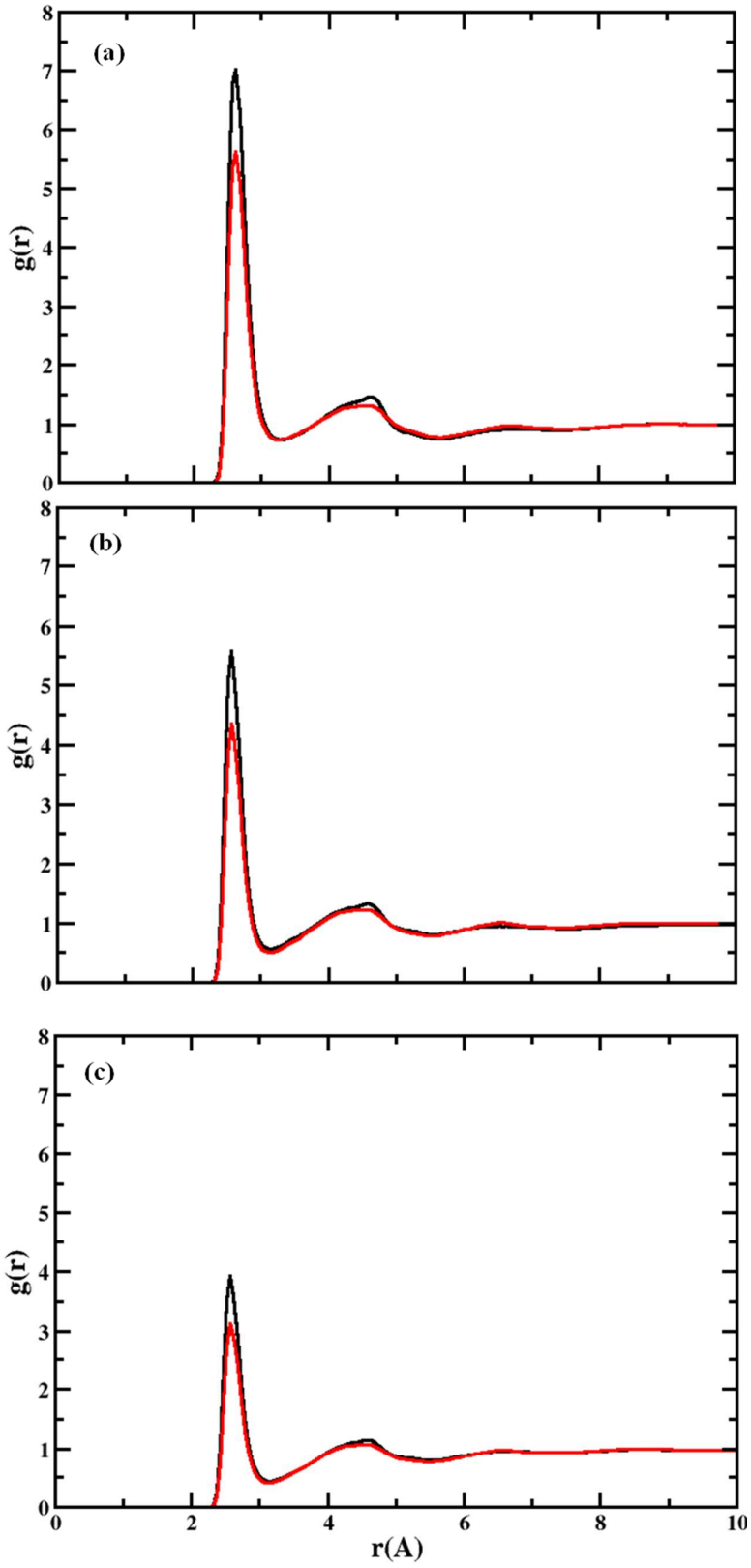

Figure 8

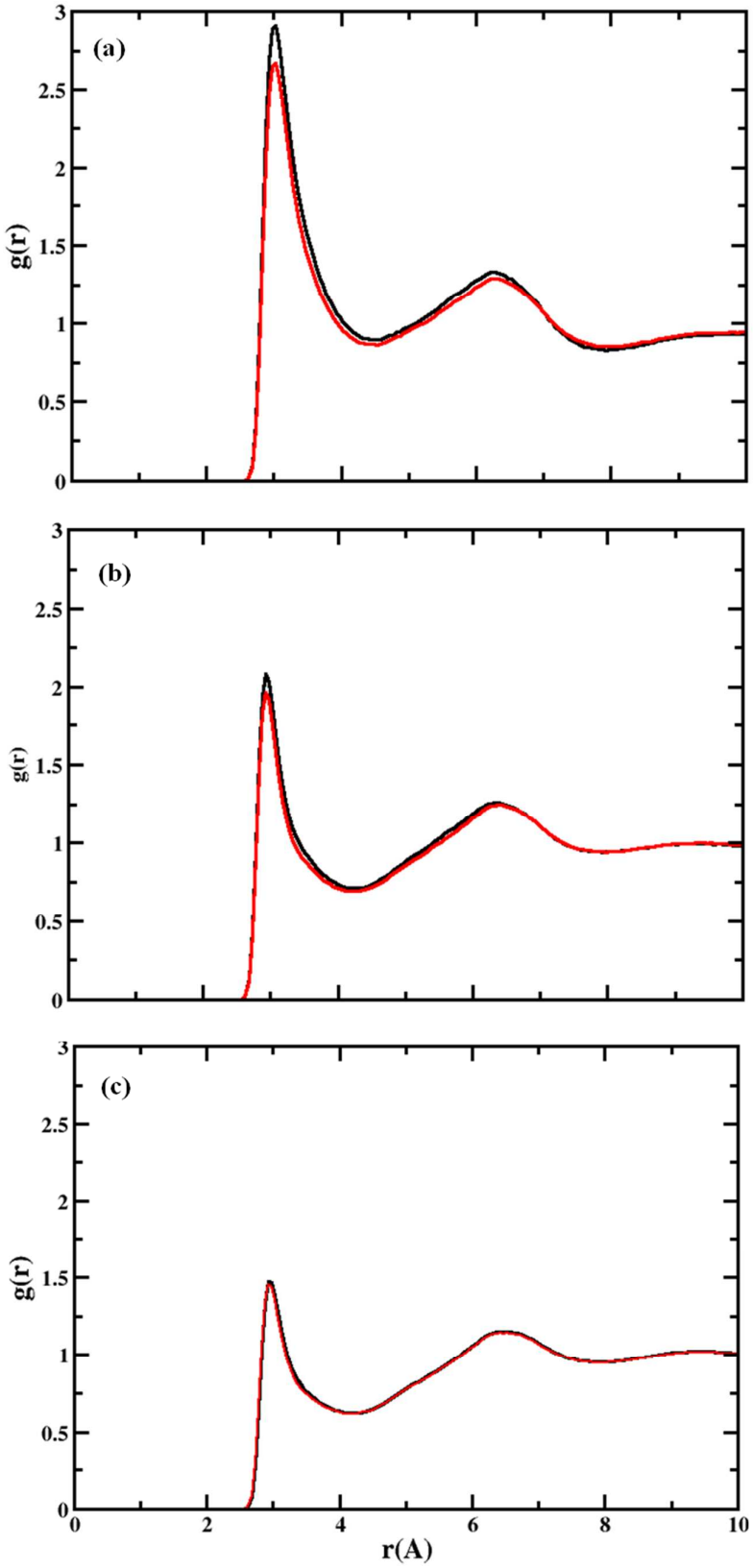

Figure 9.

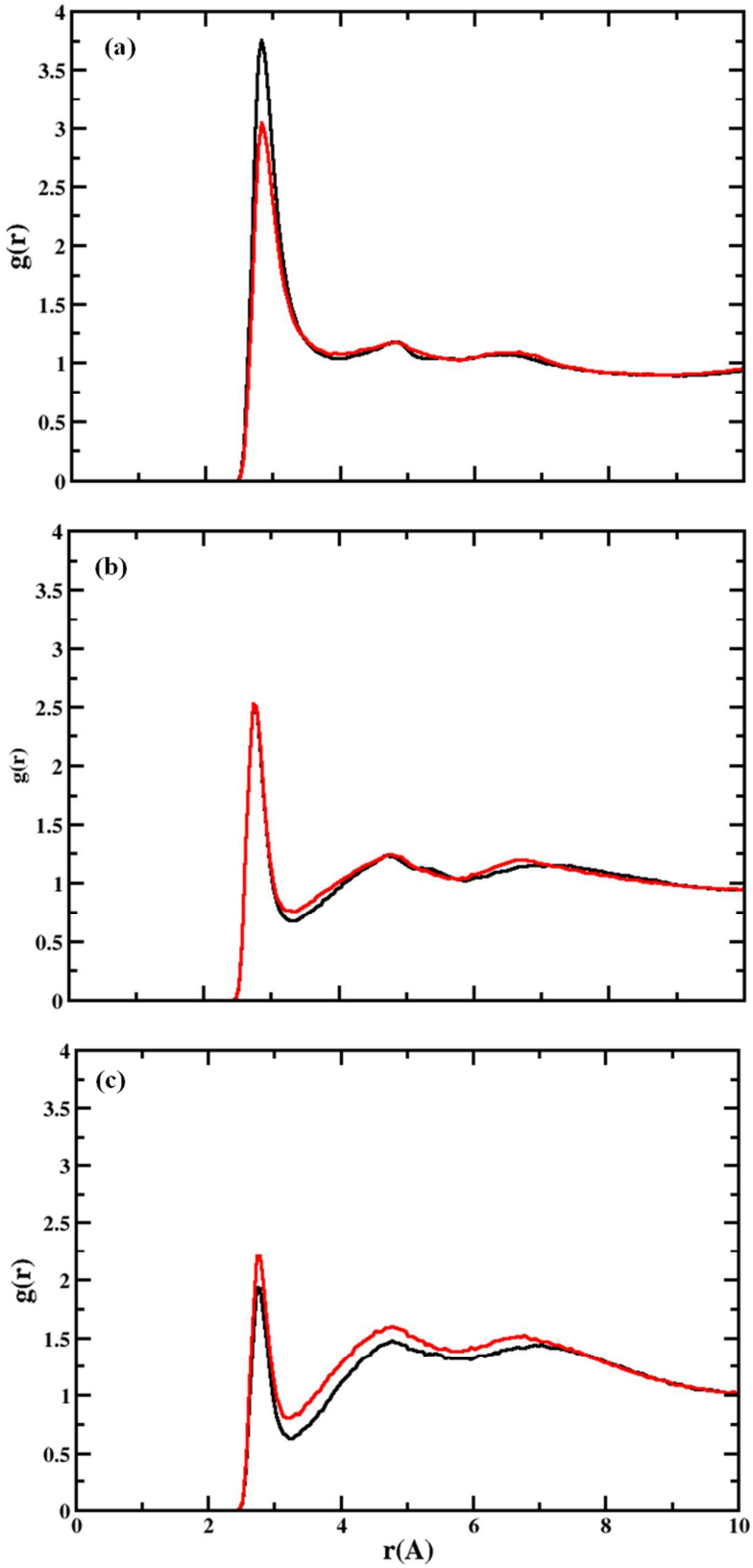

Figure 10.

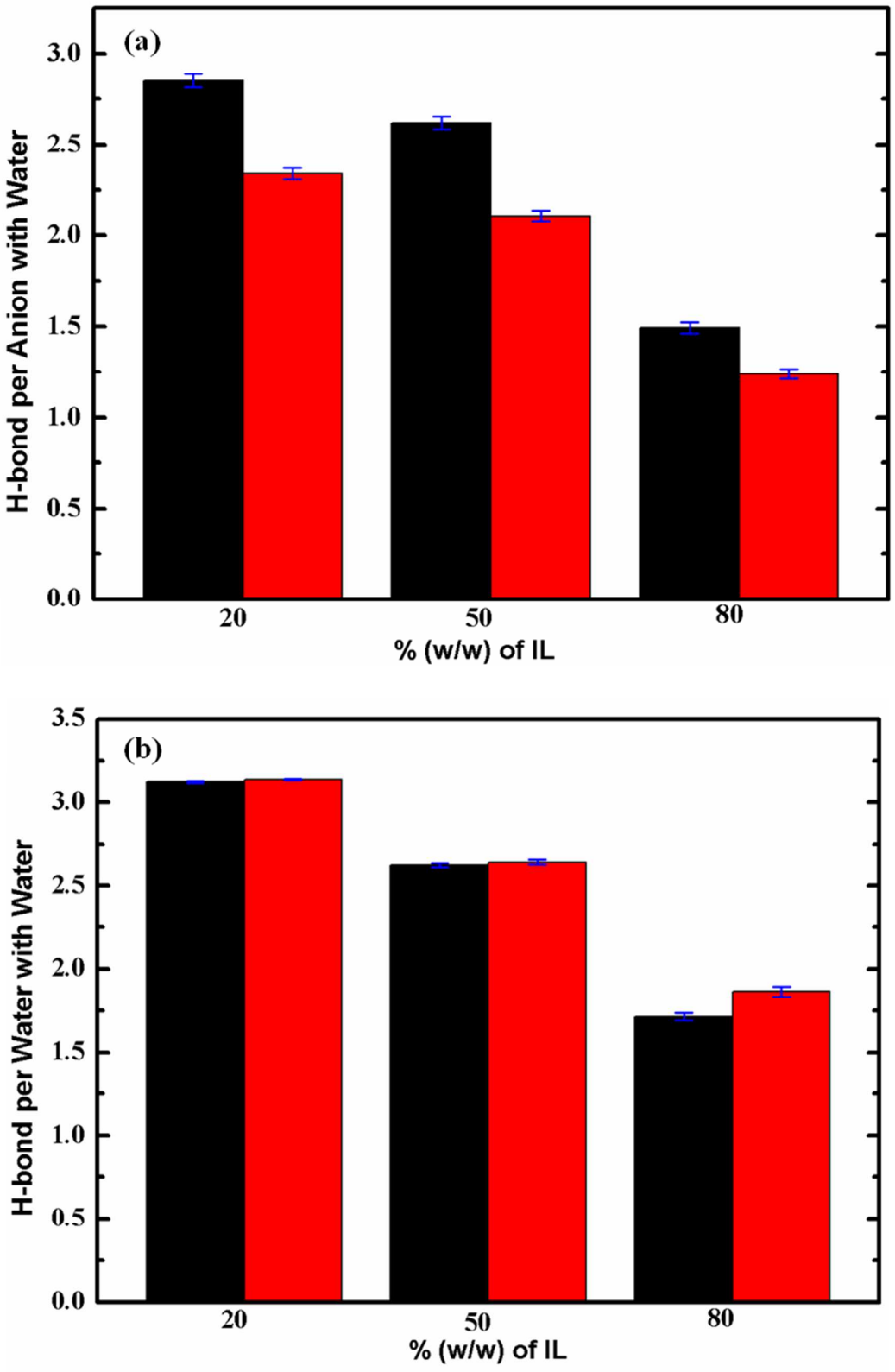

Figure 11.

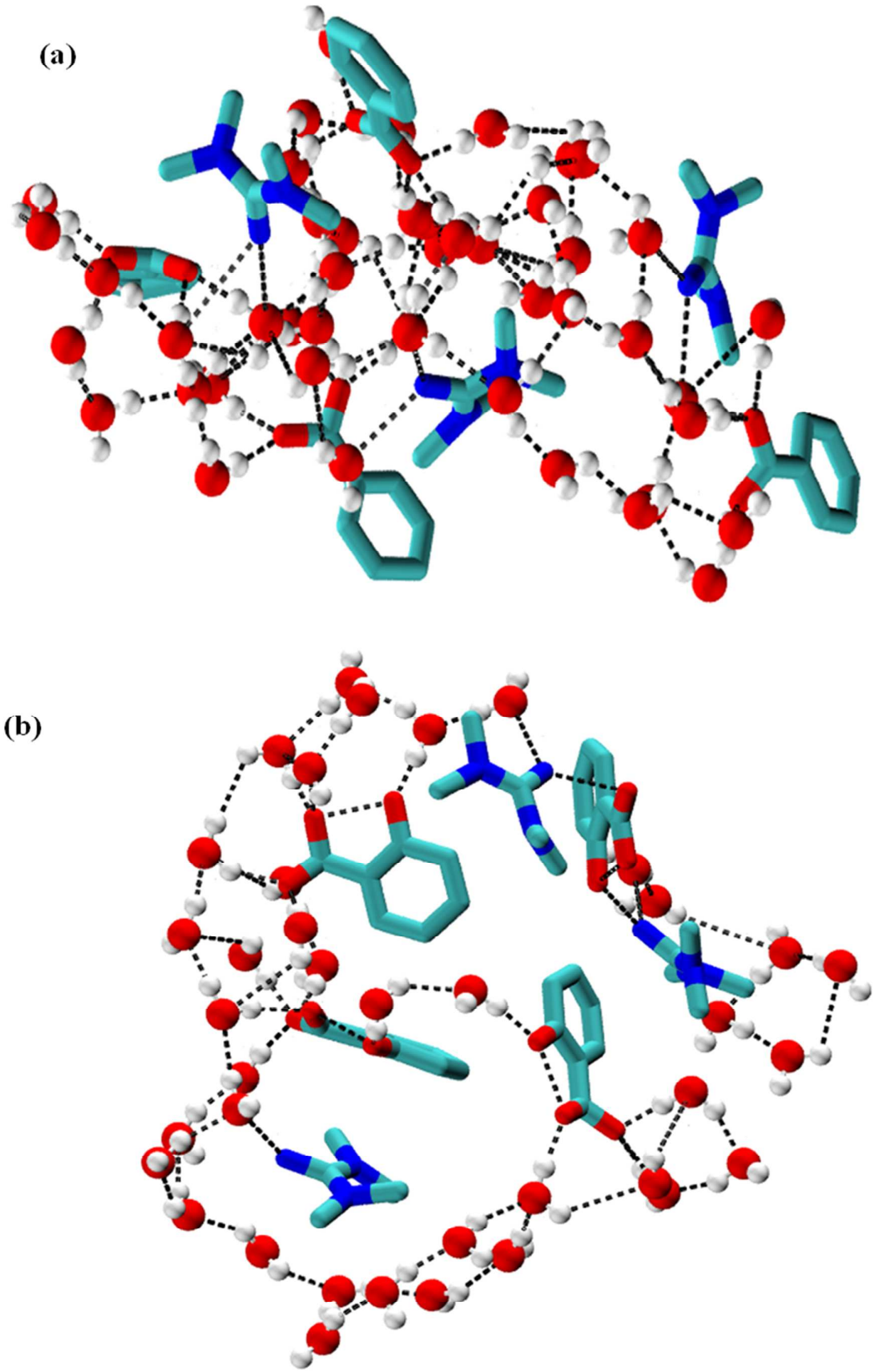

Figure 12.

Table of Contents/Abstract Graphic